PAPER

Slow crystallisation of a monodisperse foam stabilised against coarsening

Aaron J. Meagher,[ab] David Whyte,[b] John Banhart,[ac] Stefan Hutzler,*[b] Denis Weaire[b] and Francisco García-Moreno[ac]

The evolution of a three-dimensional monodisperse foam was investigated using X-ray tomography over the course of seven days. The coarsening of the sample was inhibited through the use of perfluorohexane gas. The internal configuration of bubbles is seen to change markedly, evolving from a disordered arrangement towards a more ordered state. We chart this ordering process through the use of the coordination number, the bond orientational order parameter (BOOP) and the translational order parameter.

1 Introduction

The ordering behaviour of bulk samples of equally-sized bubbles less than 1 mm in diameter—known as monodisperse microfoams—was first described somewhat incidentally by Bragg and Nye in the 1940s,[1] in the context of their work on the two-dimensional bubble raft. The latter has remained popular up to the present day,[2–4] but only recently has the nature of three-dimensional bubble crystals begun to be explored. Many key questions about their nature remain unanswered.

Optical experiments[5–7] have given only a superficial indication of structure, enough to stimulate theories that seek to explain an apparent preference for the fcc structure.[8]

The development of advanced 3D imaging techniques has been the key to structural investigation of the internal arrangements in aqueous foams. In particular, X-ray tomography has been employed with success.[9,10] While such experiments have previously been confined to synchrotron facilities, where limited experimental time can severely restrict the scope of experiments, we have shown that technological advances now allow benchtop X-ray tomography to image wet aqueous foams.[11] Initial experiments showed that the internal structure of the sample is more complicated than that of the surface layers.

In this paper, we expand upon this earlier work by investigating the ordering behaviour of a monodisperse microfoam composed of roughly 11 000 bubbles, which we image successively over the course of seven days. Through the use of perfluorohexane (PFH), the coarsening rate of the sample was lowered sufficiently for the

sample to be considered monodisperse over the course of the experiment. In addition to modifying the structure, coarsening could also lead to significant blurring in the final 3D images due to motion during the 2 hour image acquisition time.

In analysing the data, we use various measures of average and local structure, including the coordination number, the bond orientational order parameter and the translational order parameter. These metrics allow us to precisely characterise and chart the evolving structure of our foam sample. In this way, we hope to demonstrate the effectiveness of 3D monodisperse microfoams as a model system for the examination and demonstration of crystal structures and their evolution in general, just as 2D rafts have been employed ever since Bragg and Nye introduced them for that purpose.[1]

At odds with our expectation, the experiments revealed that the structure of the sample was not static over the experimental lifetime: the structure near the centre of the sample was instead seen to evolve from a disordered state on the first day of the experiment to a relatively ordered state on the seventh day. This remains surprising, since the mechanism of recrystallisation is not obvious.

2 Experimental method

Monodisperse bubbles were produced using a flow-focusing device.[6,12,13] The device is based on the co-flow of surfactant solution and pressurised gas and can produce monodisperse bubbles of diameter between 20 μm and 2.2 mm by varying the liquid flow rate, the gas pressure and outlet-nozzle diameter. For the purposes of experiment, a sample may be considered to be effectively monodisperse if the dispersity (the ratio of standard deviation to mean of the bubble diameter distribution) is less than 5%.[5] Our surfactant solution was composed of a 5% volume

[a] *Institute of Applied Materials, Helmholtz Centre Berlin for Materials and Energy, Hahn-Meitner-Platz 1, 14109 Berlin, Germany*
[b] *School of Physics, Trinity College Dublin, Dublin, Ireland. E-mail: stefan.hutzler@tcd.ie*
[c] *Technische Universität Berlin, Hardenbergstrasse 36, 10623 Berlin, Germany*

commercially-available detergent Fairy Liquid in water. This has been previously found to produce stable foams suitable for a wide variety of foam experiments. Our gas phase was formed of oxygen-free nitrogen into which the relatively insoluble compound perfluorohexane was dissolved to reduce the rate of coarsening in the foam.[14–17]

The flow-focusing device was attached to the bottom of a large rectangular box which was filled with the surfactant solution. The device was adjusted to produce monodisperse bubbles with a diameter less than 1 mm. A cubic container of side length 20 mm with one open face was placed into our surfactant solution. The container was then inverted to remove trapped air, before being positioned, open-face down, over the outlet of the device. This allowed for the bubbles produced by our flow-focusing device to be collected without exposing them to atmosphere, preventing their rapid expansion.[18] Once filled so as to produce a foam sample with approximately 12 bubble layers deep, the container was sealed by sliding a Perspex plate over the open face. The container was removed from the solution, dried, and glued to a plastic plinth which was then affixed to the rotation stage of our μCT tomographic imaging device, and allowed to settle for two hours before being imaged. Previous experiments have shown that several rearrangements occur during this settling, which would cause blurring during tomographic imaging. Note that this method of preparation is rather different from some of our earlier work, in which foam was rapidly ejected onto the surface of a pool of solution without using solid boundaries.

Each tomography took approximately two hours. The sample was removed from the device after imaging to allow other experiments to be conducted, resulting in a 22 hour period between each imaging.

Our imaging device was composed of a micro-focus 150 kV Hamamatsu X-ray source with a tungsten target. The sample was mounted on a precision rotation stage from Huber Germany; the sample's radioscopic projections were recorded using a flat panel detector C7942 (120 mm × 120 mm, 2240 × 2368 pixels, pixel size 50 μm). Different magnifications of the sample are possible by adjusting the relative distances between the X-ray source, the sample and the detector. By varying the filament voltage and current, we found that a combination of 100 kV and 100 μA provided the best contrast and lowest noise in the reconstructed foam images at high spatial resolution.

Before the third tomography, the sample was accidentally disturbed while being mounted. Only after the experiment had finished was the extent of the disturbance apparent. However, due to the startling and previously unobserved nature of the behaviour seen in the analysis, the original experimental data has been used for this publication.

X-ray tomographic reconstruction was performed using the commercially available software *Octopus*.[19] The image slices were further processed using the image processing software *MAVI*, allowing sample characteristics such as bubble volume, position *etc.*, to be extracted.[20] We approximate bubbles as spheres to obtain bubble diameters, and fit a Gaussian distribution to these to obtain a mean and standard deviation. The sample was
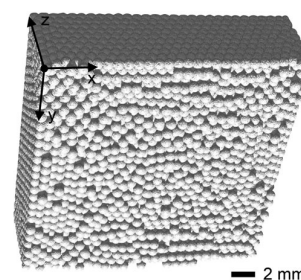

Fig. 1 Visualisation of the gas phase of the sample, showing the bottom of the sample, *i.e.* the foam–liquid interface. Gravity acts perpendicular to this surface in the z direction. Around the boundary of the foam sample, regions of hexagonal close-packed ordering are seen to occur, while the central region appears disordered.

visualised using *VGStudio MAX*.[21] A reconstruction of the foam is shown in Fig. 1.

After performing our image analysis, we disregard those objects whose diameter was outside one standard deviation of the mean associated with the bubbles of the experiment. This criterion allows us to identify the bubbles of our foam for further analysis, while ignoring most noise associated with the image segmentation process.

3 Results

On day 1 of the experiment, the average bubble diameter is 794 μm, with a dispersity of 2.4%; on day 7, the average bubble diameter is 817 μm, with a dispersity of 3.4%.

The liquid fraction of the sample was monitored by investigating the vertical X-ray absorption profile of the sample. This absorption profile may be directly related to the liquid content of the sample *via* the Beer–Lambert law.[22] Our analysis shows that the liquid fraction of the sample decreases from 0.20 to 0.18 over the course of the experiment.

While the average diameter of the bubbles of the sample did not change significantly, the internal structure underwent significant alterations. The x and y positions of the bubble centres are plotted in Fig. 2, resulting in an overlay of all foam layers.

On the first day of the experiment (Fig. 2(a)), the bubbles are seen to arrange into two distinct regions: near the container walls, linear arrangements of bubble centres are seen, while no such arrangement is seen in the sample centre. This indicates that the outer layers of the foam sample are ordered, in keeping with our previous experiments.[11] Incoherent grain boundaries are seen to form, separating the four ordered regions at the walls of the sample.

Over the lifetime of the experiment, ordered arrangements of bubbles are seen to develop in the initially disordered centre of the sample (see days 2 to 7 in Fig. 2).

To characterise the various structures and transitions which occurred within the sample over the experiment, we calculated several order metrics based on the bubble centre positions. In particular, we investigated the coordination number, n, the
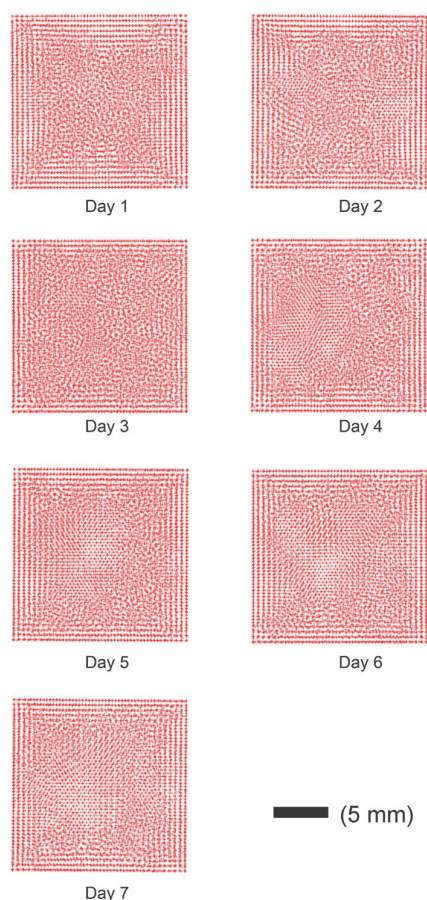
Fig. 2 Plot of the centre positions of the bubbles, projected on a horizontal plane, over the seven days. On the first day it is seen that they are arranged in parallel lines near the walls of the centre while the centre appears disordered. As the experiment progresses, the central region also becomes ordered.

translational order parameter, and the bond orientational order parameter (BOOP), as described below.

3.1 Coordination number

The local coordination number n is the number of nearest neighbours for each bubble. There exist several definitions of 'nearest neighbour', *e.g.* those objects within a packing which share a face of the corresponding Voronoi diagram,[23] or those objects within a distance corresponding to the first minimum of the radial distribution function (RDF).[24] For ease of interpretation, however, we consider two bubbles as neighbours if

$$|\vec{r}_i - \vec{r}_j| \le R_i + R_j,$$

where $\vec{r}_i$ and $\vec{r}_j$ are the positions of the ith and jth bubbles within the system, and R_i and R_j are their respective radii.

We calculate the coordination number for roughly 5000 bubbles within a cubic region at the centre of the sample, hence avoiding boundary effects. The probability distribution $P(n)$ of coordination number n over the seven days of the experiment is shown in Fig. 3. As the experiment progresses, the first broad peak, seen on day 1, evolves towards a more narrow distribution with a peak around
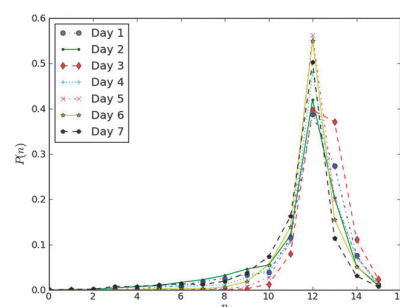

Fig. 3 Variation of the coordination number distribution over the lifetime of the experiment. The distributions have a maximum around $n = 12$, indicating close-packed ordering. The distributions on the first and third days of the experiments are wider than those of the other days.

$n = 12$. The peak widens again on the third day, following the sample's disturbance, before narrowing again over subsequent days.

3.2 Translational order parameter

The translational order parameter G is a measure of the spatial symmetry of a packing, based on the ratio of the first minimum and first maximum of the radial distribution function $g(r)$.[23] For the case of a perfectly ordered sample, $g(r)$ will be formed from a sum of δ functions. As the level of disorder increases, these δ peaks increase in width, leading to a continuous distribution. For such a distribution, G may be defined as

$$G = \left| \frac{g(r_{g1})}{g(r_{g2})} \right|$$

where r_{g1} and r_{g2} are the positions of the first minimum and first maximum of the RDF respectively. For a perfectly crystalline sample, $G = 0$. G increases as the level of translational disorder within the system increases.

Fig. 4 shows a plot of the translational order parameter as calculated over the seven days of the experiment. The values of $g(r_{g1})$ and $g(r_{g2})$ were determined from fourth-order polynomial fits to the radial distribution functions calculated from the experimental data.
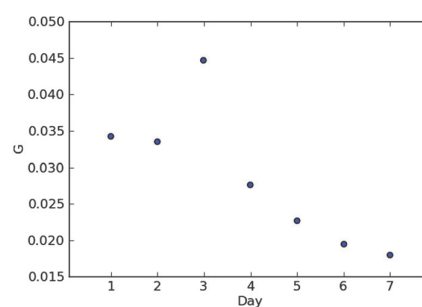

Fig. 4 Variation of the translational order parameter, G, over the seven days of the experiment, indicating the progressive ordering of the sample. The parameter is seen to decrease over the first two days of the experiment, before rising on the third day of the experiment due to a disturbance of the sample. Following this, G appears to decrease smoothly over the next five days of the experiment.

It is seen that G slightly decreases over the first two days of the experiment, before rising dramatically on the third day, corresponding to the accidental shaking of the sample. Following this, G is seen to decrease continuously for the remainder of the experiment, indicating ongoing ordering.

3.3 Analysis using bond orientational order parameter

The BOOP or Steinhardt order parameter is a measure of the local rotational order within a sample.[25] Although there exist several methods by which this rotational symmetry may be classified, it is found that Steinhardt's characterisation has proven the most useful in a variety of simulations and experiments of granular systems.[24,26] However, this type of analysis has not yet been applied to foams due to the lack of three-dimensional data of sufficiently high resolution.

The order parameter Q_ℓ for a bubble a is defined by

$$Q_\ell(a) = \sqrt{\frac{4\pi}{2\ell+1} \sum_{m=-\ell}^{\ell} \left| \frac{1}{n(a)} \sum_{b\in\text{NN}(a)} Y_{\ell m}(\theta_{ab},\phi_{ab}) \right|^2},$$

where $n(a)$ is the number of nearest neighbours, $\text{NN}(a)$ of the bubble a, ϕ_{ab} and θ_{ab} are the polar and azimuthal angles associated with the vector from a to its neighbour b, and $Y_{\ell m}$ is the spherical harmonic. The cutoff radius for classification of nearest neighbours is obtained from the first minimum of $g(r)$. Of particular relevance for us are the cases $\ell = 4$ and $\ell = 6$, which probe for cubic and hexagonal symmetry respectively.

For the hcp and fcc structures we can calculate (Q_4,Q_6) values analytically, as hcp: (0.097,0.485) and fcc: (0.191,0.574).

Some shortcomings of the BOOP method have recently been identified by Mickel *et al.* due to the strong dependence on the choice of nearest neighbours.[27] While we acknowledge the advantages of their proposed Minkowski structure method, we find that using the BOOP method is sufficient to characterise our samples: see later discussion.

Fig. 5 shows the distribution of (Q_4,Q_6) values for our sample as computed on days 1, 4 and 7. On day 1 we see a wide distribution of values, and by day 4 two peaks are visible, which become sharper by day 7. The positions of the peaks—at (0.21,0.58) and (0.14,0.50)—are close to the theoretical values for fcc and hcp structures. Visual inspection suggests that fcc is dominant; we will return to this later.

Fig. 6 shows a section excised from near the middle of the sample. Each bubble (displayed as a sphere) is coloured according to its (Q_4,Q_6) values, based on their proximity to the ideal values for fcc or hcp. We see the emergence of regions of fcc and hcp by day 7. Visually, we see that this classification is correct.

Using the same methodology, we can plot projections of the positions of all the bubbles in the sample in order to show where ordering occurs within the sample: see Fig. 7.

Both figures show that regions of fcc and hcp ordering exist in the sample. As the experiment progresses, the extent of these ordered regions increases, with a clear preference for fcc over hcp. This is more clearly demonstrated by plotting the fraction
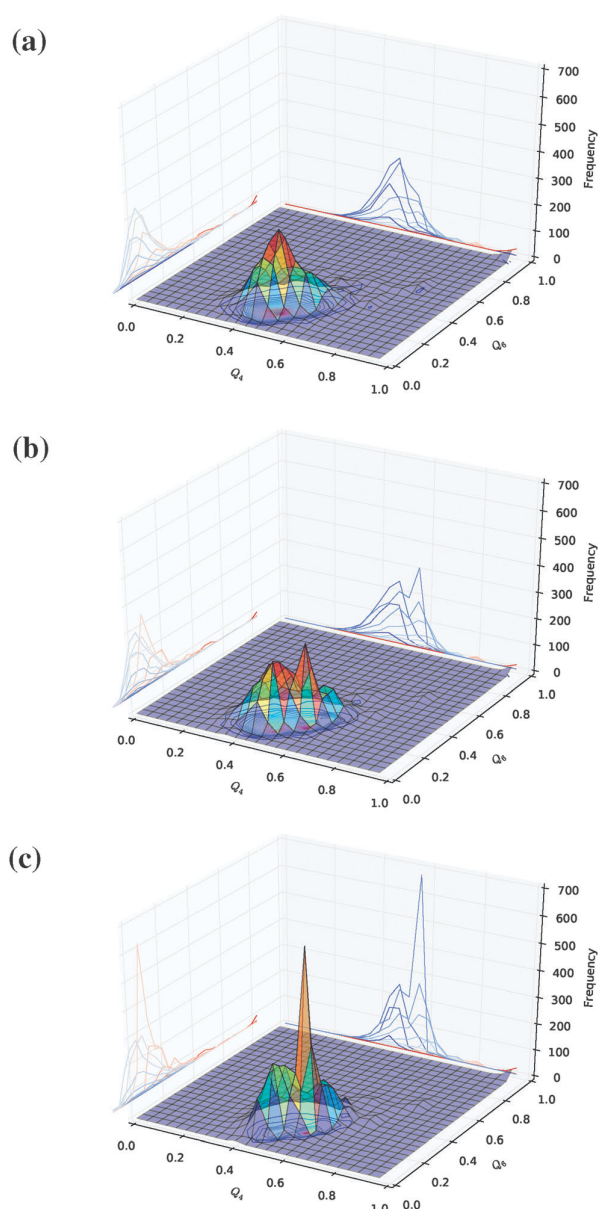

Fig. 5 3D plots showing the distribution of the Q_4 and Q_6 parameters on the (a) 1st, (b) 4th and (c) 7th days of the experiment. The wide distribution of Q_4 and Q_6 seen on the first day, (a), begins to develop into a two-peaked distribution, (b). These two peaks are centred around the Q_4 and Q_6 values associated with fcc and hcp arrangements: (0.191,0.575), and (0.097,0.485) respectively. By the seventh day of the experiment, (c), the peaked distribution has continued to develop a clear preference for the fcc structure, indicated by the relative increase in the height of this peak relative to that of the hcp structure.

of bubbles classified as either fcc or hcp over time, as in Fig. 8. On day 1, $\sim$12% of the bubbles are hcp-ordered, and $\sim$15.6% are fcc-ordered, with a ratio $N_{\text{fcc}}/N_{\text{hcp}} \approx 1.3$, in line with previous experiments.[6,7] The fraction of fcc bubbles increases over time, while that of hcp remains roughly constant; by day 7, $\sim$10% are hcp and $\sim$26% are fcc, with $N_{\text{fcc}}/N_{\text{hcp}} \approx 2.5$.
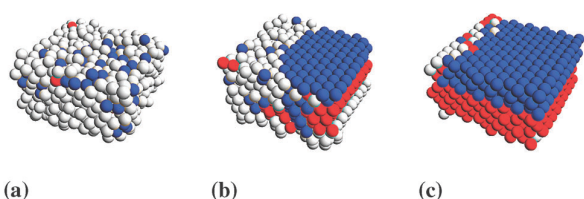
Fig. 6 Bubbles excised from near the centre of the sample on days 1, 4 and 7 respectively. These bubbles are coloured according to their (Q_4,Q_6) values: red for fcc, blue for hcp, white for other.
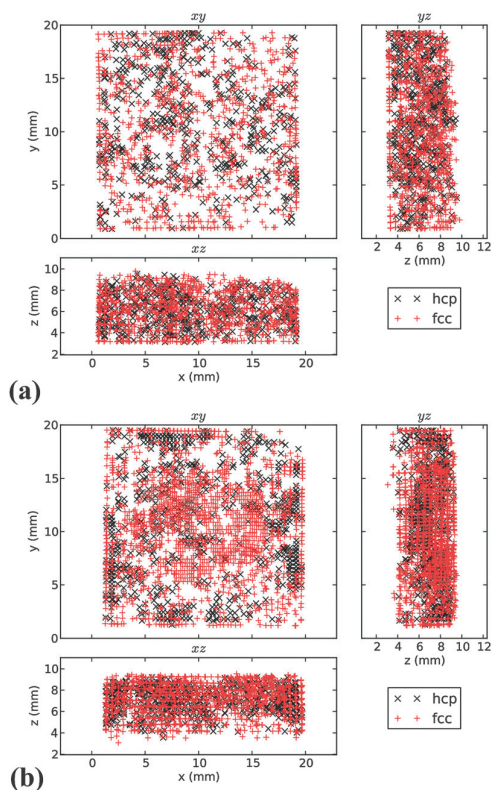

Fig. 8 Plot showing the variation of the ratios N_{fcc}/N_{total} and N_{hcp}/N_{total}. The fraction of hcp ordering remains roughly constant, while the fraction of fcc ordering rises.

Fig. 7 Plot showing the distribution of fcc- (red +) and hcp- (black ×) ordered regions within the foam sample on days (a) 3 and (b) 7 of the experiment. Views of the xy, yz and xz planes are displayed. The extent of the crystallisation areas is seen to increase, but no clear distinction between areas of fcc and hcp ordering occurs.

4 Discussion

As reported in Section 3, the average bubble diameter increases by approximately 3% over the 7 days of the experiment. Despite this very small increase, the dispersity of the sample never rises above 5%, the conventional limit for a monodisperse foam.[5]

Previous experiments on 3D foams formed without the addition of a low-solubility gas phase have shown a significantly higher coarsening rate,[28] so we can conclude that the PFH has indeed reduced the coarsening of the foam.

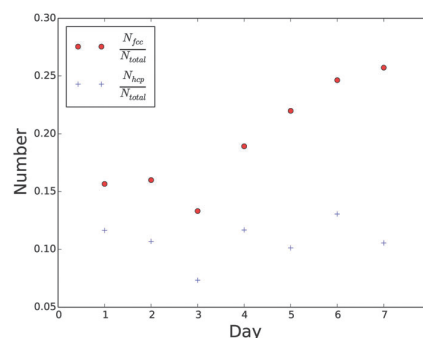Each order parameter calculated indicates the ongoing ordering process occurring within the sample.

This is first shown by the hexagonal patterns present within the xy plots of centre positions (Fig. 2). The regular arrangement of points near the border of the sample indicate crystalline structures in these areas, while the lack of such arrangements near the centre of the sample suggest that this region is disordered. The exact nature of this crystallisation is determined by BOOP analysis. This clearly shows that the crystalline regions are composed of fcc and hcp regions. The initial preference for fcc over hcp is in keeping with theoretical discourse about mechanical stability;[8] this preference becomes stronger over the seven days, as indicated by the increased prevalence of the BOOP signature of fcc over that of hcp.

It must be noted, however, that the BOOP signatures of fcc and hcp ordering within our sample are shifted slightly with respect to the values associated with their ideal values. We suspected that this shift was due to the finite compressibility of our bubbles. To investigate the validity of this assumption, we calculated the BOOP signature associated with a deformed fcc structure: namely, the BOOP of an fcc lattice in which the lattice spacing in the $\langle 100 \rangle$ direction has been successively reduced. We found that, as the compression of the sample increased, the corresponding BOOP values spread in a similar way to those found in experiment. xy plots of the regions of fcc and hcp ordering show no clear spatial preference for finding either fcc or hcp.

The coordination number of the sample shows that ordering occurs as the distribution of n narrows. The probability of bubbles having 13 neighbours or more is in keeping with previous experiments on deformable spheres with packing fractions above 0.74.[29]

The translational order parameter, G, may be used to examine the rate of crystallisation within the sample. Over the last 5 days of the experiment, the decreasing rate of change of G indicates that the rate of structural change is also decreasing. This is to be expected as the region of disorder decreases in size.

The driving force behind this crystallisation is still undetermined. Coarsening dynamics have previously been linked to relaxation dynamics. However, the significantly reduced coarsening rate within our foam suggests that coarsening cannot be the main source of the structural rearrangements

here, although it may be one of several contributing factors. In addition, the increased ordering of the foam following physical disturbance of the sample is incongruent with such coarsening arguments. We believe that thermal fluctuations in the laboratory over a 24 hour period could contribute to the behaviour observed: a difference of a few degrees between day and night temperatures would result in a change in the volume of the bubbles of a few percent: this repeated expansion and contraction may provide the mechanical force necessary for the rearrangements.

The drainage of the sample may also be implicit in this ordering process. Liquid drainage has been previously linked to local rearrangements of bubbles.[30,31] In addition, as the shear modulus of a foam is inversely proportional to its liquid fraction, drainage should result in rearrangements becoming more difficult over time, resulting in a reduction in the crystallisation rate, as we see from the translational order parameter.

5 Conclusions

We see that the PFH and nitrogen gas mixture produces a foam whose coarsening rate is such that it remains monodisperse over the course of a week. In spite of this, the internal structure of the sample is seen to change dramatically and unexpectedly during this time, progressing from a disordered to a more ordered state. The slow rate of this ordering was surprising, as the prevailing opinion has been that this was a rapid process, occurring directly after crystallisation.

The slow rate of this process allows it to be easily imaged using convenient lab-based X-ray tomography. From this data, the coordination number, translational order parameter and BOOP have all been shown as useful metrics for charting this process. We see that the foam produces regions of fcc and hcp ordering, with a clear preference for fcc crystallisation.

Now that we have shown that dynamic crystalline processes may be imaged using lab-based tomography, a much broader range of experiments may be conducted. We will be able to see how boundary conditions, crystal defects and other anomalies influence the crystallisation of these foams. In this way, we will fully expand the original work of Bragg and Nye[1] into three dimensions, employing their bubble model as a dynamic model of 3D crystal structures.

Acknowledgements

References

1 L. Bragg and J. Nye, *Proc. R. Soc. London, Ser. A*, 1947, 474–481.

2 J. Georges, G. Meille, J. Loubet and A. Tolen, *Nature*, 1986, **320**, 342–344.

3 A. Gouldstone, K. J. Van Vliet and S. Suresh, *Nature*, 2001, **411**, 656.

4 K. Van Vliet and S. Suresh, *Philos. Mag. A*, 2002, **82**, 1993–2001.

5 R. Höhler, Y. Yip Cheung Sang, E. Lorenceau and S. Cohen-Addad, *Langmuir*, 2008, **24**, 418–425.

6 A. Van der Net, W. Drenckhan, D. Weaire and S. Hutzler, *Soft Matter*, 2006, **2**, 129–134.

7 A. van der Net, G. W. Delaney, W. Drenckhan, D. Weaire and S. Hutzler, *Colloids Surf., A*, 2007, **309**, 117–124.

8 S. Heitkam, W. Drenckhan and J. Fröhlich, *Phys. Rev. Lett.*, 2012, **108**, 148302.

9 J. Lambert, I. Cantat, R. Delannay, R. Mokso, P. Cloetens, J. A. Glazier and F. m. c. Graner, *Phys. Rev. Lett.*, 2007, **99**, 058304.

10 A. Stocco, F. Garcia-Moreno, I. Manke, J. Banhart and D. Langevin, *Soft Matter*, 2011, **7**, 631–637.

11 A. Meagher, M. Mukherjee, D. Weaire, S. Hutzler, J. Banhart and F. Garcia-Moreno, *Soft Matter*, 2011, **7**, 9881–9885.

12 A. M. Ganán-Calvo and J. M. Gordillo, *Phys. Rev. Lett.*, 2001, **87**, 274501.

13 C. S. Smith, *J. Appl. Phys.*, 1949, **20**, 631.

14 F. G. Gandolfo and H. L. Rosano, *J. Colloid Interface Sci.*, 1997, **194**, 31–36.

15 V. Carrier, S. Destouesse and A. Colin, *Phys. Rev. E: Stat., Nonlinear, Soft Matter Phys.*, 2002, **65**, 061404.

16 A. Saint-Jalmes, Y. Zhang and D. Langevin, *Eur. Phys. J. E: Soft Matter Biol. Phys.*, 2004, **15**, 53–60.

17 D. Weaire and V. Pageron, *Philos. Mag. Lett.*, 1990, **62**, 417–421.

18 M. Fortes and A. Deus, *J. Colloid Interface Sci.*, 1995, **176**, 248–255.

19 M. Dierick, B. Masschaele and L. Van Hoorebeke, *Meas. Sci. Technol.*, 2004, **15**, 1366.

20 *Fraunhofer ITWM, Kaiserslautern*, 2005.

21 Information available at http://www.volumegraphics.com/products/vgstudio-max/.

22 F. Garcá-Moreno, S. Tobin, M. Mukherjee, C. Jiménez, E. Solórzano, G. V. Kumar, S. Hutzler and J. Banhart, *Soft Matter*, 2014, **10**, 6955–6962.

23 J. Olafsen, *Experimental and Computational Techniques in Soft Condensed Matter Physics*, Cambridge University Press, 2010.

24 T. Aste, M. Saadatfar and T. Senden, *Phys. Rev. E: Stat., Nonlinear, Soft Matter Phys.*, 2005, **71**, 061302.

25 P. J. Steinhardt, D. R. Nelson and M. Ronchetti, *Phys. Rev. B: Condens. Matter Mater. Phys.*, 1983, **28**, 784.

26 W. Lechner and C. Dellago, *J. Chem. Phys.*, 2008, **129** 114707.

27 W. Mickel, S.C. Kapfer, G. E. Schröder-Turk and K. Mecke, *J. Chem. Phys.*, 2013, **138**, 044501, DOI: 10.1063/1.4774084.

28 C. Gonatas, J. Leigh, A. Yodh, J. A. Glazier and B. Prause, *Phys. Rev. Lett.*, 1995, **75**, 573.

29 S. Mukhopadhyay and J. Peixinho, *Phys. Rev. E: Stat., Nonlinear, Soft Matter Phys.*, 2011, **84**, 011302.

30 V. Carrier and A. Colin, *Langmuir*, 2003, **19**, 4535–4538.

31 A. Gopal and D. Durian, *Phys. Rev. Lett.*, 2003, **91**, 188303.